

Geodynamo and mantle convection simulations on the Earth Simulator using the Yin-Yang grid

Akira Kageyama and Masaki Yoshida

The Earth Simulator Center, Japan Agency for Marine-Earth Science and Technology,
Showa-machi 3173-25, Yokohama, Japan

E-mail: kage@jamstec.go.jp

Abstract. We have developed finite difference codes based on the Yin-Yang grid for the geodynamo simulation and the mantle convection simulation. The Yin-Yang grid is a kind of spherical overset grid that is composed of two identical component grids. The intrinsic simplicity of the mesh configuration of the Yin-Yang grid enables us to develop highly optimized simulation codes on massively parallel supercomputers. The Yin-Yang geodynamo code has achieved 15.2 Tflops with 4096 processors on the Earth Simulator. This represents 46% of the theoretical peak performance. The Yin-Yang mantle code has enabled us to carry out mantle convection simulations in realistic regimes with a Rayleigh number of 10^7 including strongly temperature-dependent viscosity with spatial contrast up to 10^6 .

1. Introduction

The Earth (radius $r = 6400\text{km}$) is composed of three spherical layers; the inner core ($r = 1200\text{km}$), the outer core ($r = 3500\text{km}$), and the mantle. Computer simulations of the Earth's interior need efficient spatial discretization methods in the spherical shell geometry. To achieve high sustained performance on massively parallel supercomputer such as the Earth Simulator, spatially localized discretization methods rather than spectral methods are desirable. Recently, we proposed a new spherical grid system, the "Yin-Yang grid," for geophysical simulations. Because there is no grid mesh that is orthogonal over the entire spherical surface and, at the same time, free of coordinate singularity or grid convergence, we have chosen an overset grid approach. A spherical surface is decomposed into two identical subregions. The decomposition (or dissection) enables us to cover each subregion by a grid system that is individually orthogonal and singularity-free. Each component grid in this Yin-Yang grid is a low latitude component of the usual latitude-longitude grid on the spherical polar coordinates (90 degree about the equator and 270 degree in the longitude). Therefore, the grid spacing is quasi-uniform and the metric tensors are simple and analytically known. One can directly apply mathematical and numerical resources that have been written in the spherical polar coordinates or latitude-longitude grid. Since the two component grids are identical and they are combined in a complementary way, various routines of the code can be recycled twice for each component grid at every simulation time step. We have developed finite difference codes based on the Yin-Yang grid for (i) the geodynamo simulation in the outer core, and (ii) the mantle convection simulation.

In general, a dissection of a computational domain generates internal borders or internal boundaries between the subregions. In the overset grid methodology [1], the subregions are

permitted to partially overlap one another on their borders. The overset grid is also called as overlaid grid, or composite overlapping grid, or Chimera grid [2]. The validity and importance of the overset approach in the aerodynamical calculations was pointed out by Steger [3]. Since then this method is widely used in this field. It is now one of the most important grid techniques in the computational aerodynamics.

In the computational geosciences, the idea of the overset grid approach appeared rather early. Phillips proposed a kind of composite grid in 1950's to solve partial differential equations on a hemisphere, in which the high latitude region of the latitude-longitude grid is "capped" by another grid system that is constructed by a stereographic projection to a plane on the north pole [4, 5, 6]. After a long intermission, the overset grid method seems to attract growing interest in geoscience these days. The "cubed sphere" [7] is an overset grid that covers a spherical surface with six component grids that correspond to six faces of a cube. The "cubed sphere" is recently applied to the mantle convection simulation [8]. In the atmospheric research, other kind of spherical overset grid is used in a global circulation model [9], in which the spherical surface is covered by two component grids—improved stereographic projection grids—in northern and southern hemispheres that overlap in the equator.

Among indefinite variations of spherical overset grid systems, what is the simplest one? In general, the structure of a spherical overset grid is largely determined by the number of divided pieces of the sphere n (≥ 2). Here we consider the minimum case of $n = 2$, i.e., the spherical dissections by two pieces. One can divide a sphere into two parts, for example, by cutting along a small circle at any latitude. We concentrate on a special class of $n = 2$ dissections in which the two pieces are geometrically identical, i.e., they have exactly same size and shape. Another condition we impose here to maximize the simplicity is the symmetry of the piece. It should have two fold symmetry in two perpendicular directions; up-down and right-left. Here we call this special class of dissections as yin-yang dissection of a sphere.

A trivial example of the yin-yang dissection is obtained by cutting along the equator or any great circle, producing two hemispheres.

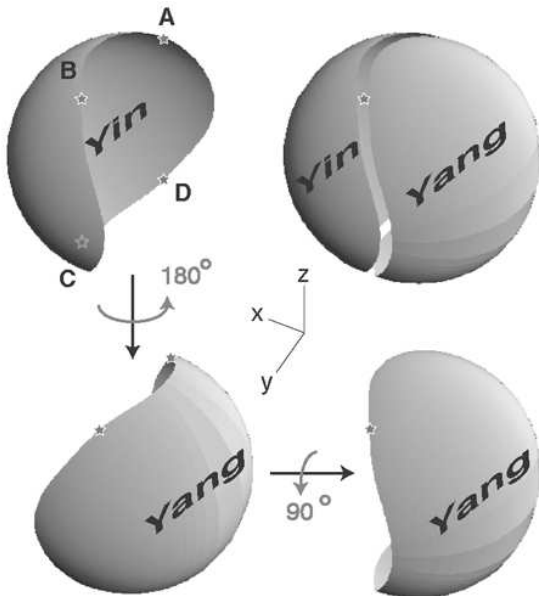


Figure 1. An example of yin-yang dissection of a sphere: A sphere is divided into two identical pieces, with same shape and size. Each piece has two fold symmetry; up-down and right-left. They are combined in a complementary way to cover a spherical surface. The two identical pieces of the yin-yang dissection is transformed each other by two successive rotations, or one rotation.

Other yin-yang dissections are obtained by modifying the cut curve from the great circle. Let S_{yin} be a piece of a sphere S with radius $r = \sqrt{2}$. We should keep the surface area of S_{yin} being $2\pi r^2$, just a half of S 's surface. An example of S_{yin} is shown in the upper left panel in Fig. 1.

The border curve of S_{yin} passes through the following four points on the sphere; point A at $(x, y, z) = (0, -1, +1)$, B at $(0, +1, +1)$, C at $(0, +1, -1)$ and D at $(0, -1, -1)$. The curve AB , between A and B , is arbitrarily as long as it is symmetric about the $y = 0$ plane. Other three curves, BC , CD , and DA , are uniquely constructed from the curve AB as follows: The curve BC is a copy of AB followed by two successive rotations, first 180 degree about the z axis, then 90 degree about the x axis. The curve CD is the mirror image of AB about $z = 0$ plane. The curve DA is the mirror image of BC about $y = 0$ plane. From this definition of the border curve $ABCD$, it is obvious that the surface area of S_{yin} is just a half of that of the sphere S . Now we make a copy of S_{yin} and call it S_{yang} which is rotated for 180° around z -axis. (See lower left panel of Fig. 1.) Then, rotate it again, but this time for 90° degree around x -axis, as shown in the lower right panel. Then the original piece S_{yin} (the upper left) and the rotated copy S_{yang} (the lower right) can be combined, and they just cover the original sphere S as shown in the upper right in this figure. This is an constructive illustration of the yin-yang dissection of a sphere.

Since the initial curve AB was arbitrarily, it is obvious that there are indefinite variations of the yin-yang dissection of the sphere S .

2. Yin-Yang grids

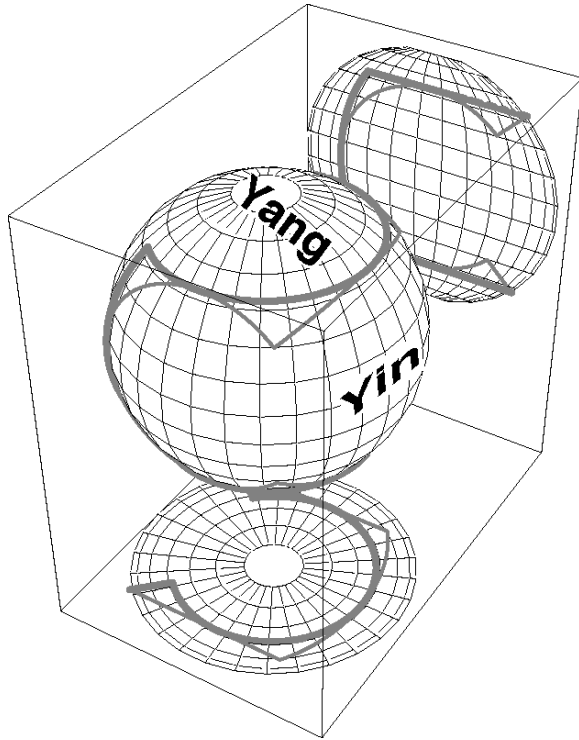


Figure 2. A dissection of a sphere into two identical pieces—Yin and Yang—with a partial overlap. The thick and thin curves are the borders of Yin and Yang piece, respectively. The thick curve (Yin's border) is always located in either constant latitudes or constant longitudes. The Yin (Yang) piece is a rectangle in the computational (θ, ϕ) space of the Yin (Yang) grid.

The overset grid methodology gives us a freedom to design the shape of the component grid as long as the grids has *minimum* overlap one another [1]. Therefore, we can take the component grid as a rectangle in the computational (θ, ϕ) space. Fig. 2 shows a spherical dissection by two identical pieces with partial overlap. The Yin piece is surrounded by a thick red curve and Yang piece is surrounded by a thin curve. Note that the northern and southern borders of the Yin piece are located in constant latitudes and the western and eastern borders are located in constant longitudes. In other words, the Yin piece in Fig. 2 is a rectangle in the (θ, ϕ) space of the Yin's spherical coordinates, and therefore, the Yang piece is also (the same) rectangle

in Yang's coordinates that is perpendicular to the Yin's. The Yin-Yang grid based on this partially overlapped spherical dissection is shown in Fig. 3. Here, each component grid spans the subregion S_y defined by

$$S_y := \{\theta, \phi\}, \quad |\theta - \pi/2| \leq \pi/4 + \delta, \quad |\phi| \leq 3\pi/4 + \delta, \quad (1)$$

with a small buffer δ which is necessary to keep the minimum overlap between Yin and Yang. Note that in the simulation code, one subroutine for the fluid solver, for instance, can be recycled twice because the grid distribution is exactly the same for the Yin and Yang.

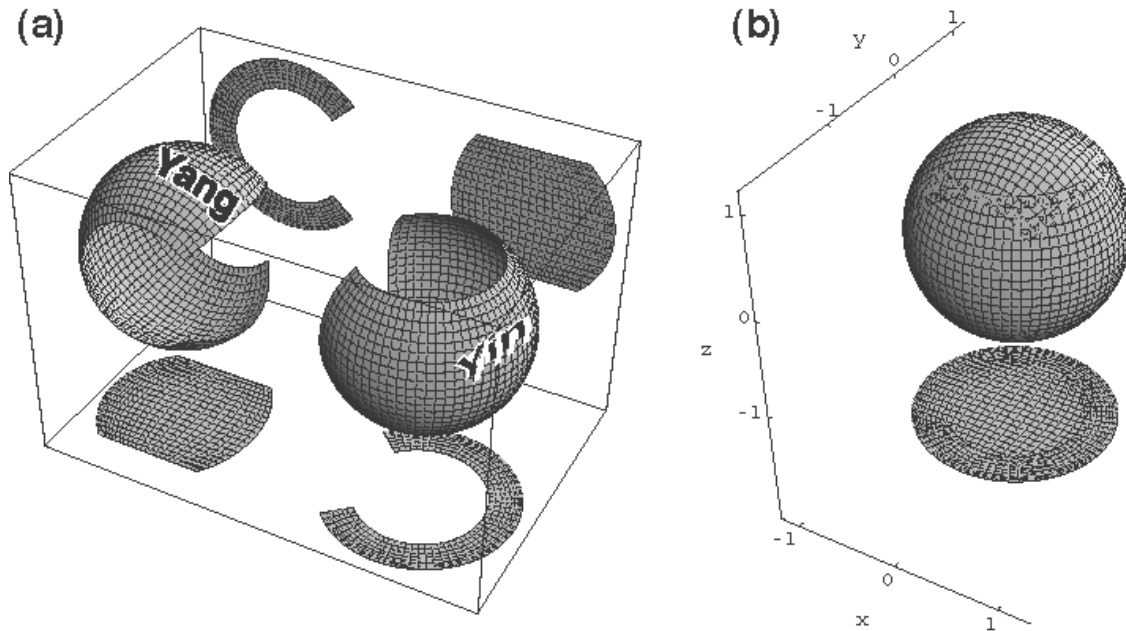


Figure 3. A Yin-Yang grid based on the yin-yang dissection with partial overlap shown in Fig. 2. Each component grid is rectangle in the computational (θ, ϕ) space.

The Yin and Yang are converted each other by a rotation. The Yin's cartesian coordinates x_i^n for $i = 1, 2, 3$ and that Yang's coordinates x_i^e are related by

$$x_i^e = M_{ij} x_j^n \quad \text{for } i, j = 1, 2, 3 \quad (2)$$

where $M_{11} = -1$, $M_{23} = M_{32} = 1$, and $M_{ij} = 0$ for other components. Note that the matrix M satisfies

$$M = M^t = M^{-1}, \quad (3)$$

which indicates a complementary relation between the Yin and Yang. The coordinate transformation from Yin to Yang is mathematically the same as that from Yang to Yin. This enables us to make only one, instead of two, subroutines that involve any data transformation between Yin and Yang, which is required in the mutual interpolation for the internal boundary condition on the overset grid borders.

The transformation formula of any vector components $\mathbf{v} = (v_r, v_\theta, v_\phi)$ between Yin and Yang is given by

$$\begin{pmatrix} v_r^e \\ v_\theta^e \\ v_\phi^e \end{pmatrix} = P \begin{pmatrix} v_r^n \\ v_\theta^n \\ v_\phi^n \end{pmatrix}, \quad (4)$$

with the transformation matrix

$$P = \begin{pmatrix} 1 & 0 & 0 \\ 0 & -\sin \phi^e \sin \phi^n & -\cos \phi^n / \sin \theta^e \\ 0 & \cos \phi^n / \sin \theta^e & -\sin \phi^e \sin \phi^n \end{pmatrix}. \quad (5)$$

The inverse transformation is given by the same matrix; $P^{-1} = P$, which is another reflection of the complementary nature between the Yin and Yang.

Another merit of the Yin-Yang grid resides in the fact that the component grid is nothing but (a part of) the latitude-longitude grid. We can directly deal with the equations to be solved with the usual spherical polar coordinates. The analytical forms of metric tensors are familiar in the spherical coordinates. We can directly code the basic equations in the program as they are formulated in the spherical coordinates. We can make use of various resources of mathematical formulas, program libraries, and other tools that have been developed in the spherical polar coordinates.

In order to illustrate the programming strategy in the Yin-Yang method, let us consider a two-dimensional fluid problem on a sphere S . Suppose that two components of the flow velocity $\mathbf{v} = (v_\theta, v_\phi)$ and the pressure p are written in `vel_t`, `vel_p`, and `press` in a Fortran 90/95 program. They can be combined into one structure or “type” in Fortran 90/95 as

```
type fluid_
  real(DP), dimension(NT,NP) :: vel_t, vel_p, press
end type fluid_
```

where `NT`, `NP` are the grid size integers in θ and ϕ directions in the subregion S_y of eq. (1). Using this structured type, we declare two variables for the fluid; one is for Yin and another for Yang:

```
type(fluid_) :: fluid_yin, fluid_yang
```

Then, we call a fluid solver subroutine, here named `navier_stokes_solver`, that numerically solves the Navier-Stokes equation in the spherical coordinates in the subregion S_y :

```
call navier_stokes_solver(fluid_yin)
call navier_stokes_solver(fluid_yang)
```

The first call of `navier_stokes_solver` solves the fluid motion in the S_y region defined in the Yin’s spherical coordinates and the second call is for the same region S_y defined in the Yang’s coordinates. But in the program code, we do not have to distinguish the two S_y regions since the basic equations, numerical grid distribution, and therefore, all numerical tasks are identical in the computational space. For a rotating fluid problem with a constant angular velocity $\boldsymbol{\Omega}$, we have the Coriolis force term in the Navier-Stokes equation that seems to break the symmetry between the Yin grid and Yang grid, but it is still possible to write the equation in exactly the same form for the Yin and Yang grids by explicitly writing three components of angular velocity in the Coriolis force term $2\mathbf{v} \times \boldsymbol{\Omega}$ in the subroutine. Then, we call the routine with the angular velocity vector in each grid (Yin or Yang) as the second argument:

```
call navier_stokes_solver(fluid_yin,omega_yin)
call navier_stokes_solver(fluid_yang,omega_yang)
```

where `omega_yin` and `omega_yang` are again structured variables that hold three components of the $\boldsymbol{\Omega}$ vector: For example, `omega_yin` holds three components of cartesian vector components in the Yin grid $(\Omega_x^n, \Omega_y^n, \Omega_z^n) = (0, 0, \Omega)$, and `omega_yang` holds $(\Omega_x^e, \Omega_y^e, \Omega_z^e) = (0, \Omega, 0)$.

Our experience tells that it is easy to convert an existing latitude-longitude based program into a Yin-Yang based program since there are many shared routines between them. In addition to that the size of the code as well as its complexity is drastically reduced by the code conversion because we can remove routines that are designed to resolve the pole problems on the latitude-longitude grid.

3. Application to the mantle convection simulation

3.1. Simulation model

We applied the Yin-Yang grid described in the previous section for the mantle convection simulation. The details of the adopted numerical methods and benchmark tests can be found in [10].

We model the mantle convection as a thermal convection of a Boussinesq fluid with infinite Prandtl number heated from bottom of a spherical shell [11]. The ratio of the inner radius ($r = r_0$) and the outer radius ($r = r_1$) is 0.55. The normalization factors for the non-dimensionalization of the length, velocity, time and temperature are \hat{d} , $\hat{\kappa}/\hat{d}$, $\hat{d}^2/\hat{\kappa}$ and $\Delta\hat{T} = \hat{T}_{bot} - \hat{T}_{top}$, respectively, where d is the thickness of the shell, $\hat{\kappa}$ the thermal diffusivity, and \hat{T}_{bot} and \hat{T}_{top} are the temperatures on the bottom and top surfaces. The hat stands for dimensional quantity. The non-dimensional equations of mass, momentum, and energy conservation governing the thermal convection are,

$$\nabla \cdot \mathbf{v} = 0, \quad (6)$$

$$0 = -\nabla p + \nabla \cdot (\mu \dot{\mathbf{e}}) + RaT\hat{\mathbf{r}}, \quad (7)$$

$$\frac{\partial T}{\partial t} = \nabla^2 T - \mathbf{v} \cdot \nabla T + H, \quad (8)$$

where \mathbf{v} is the velocity vector, p pressure, μ viscosity, T temperature, t time, $\dot{\mathbf{e}}$ strain-rate tensor, and $\hat{\mathbf{r}}$ is the unit vector in the r -direction. The Rayleigh number is defined by

$$Ra \equiv \frac{\hat{\rho}\hat{g}\hat{\alpha}\Delta\hat{T}\hat{d}^3}{\hat{\kappa}\hat{\mu}}, \quad (9)$$

where $\hat{\rho}$ is the density, \hat{g} the gravitational acceleration, and $\hat{\alpha}$ is the thermal expansivity. Most of the heat for Earth's mantle comes from a combination of radioactive decay of isotopes and secular cooling of the mantle. The internal heating is defined by

$$H \equiv \frac{\hat{Q}\hat{d}^2}{\hat{\kappa}\hat{c}_p\Delta\hat{T}}, \quad (10)$$

where \hat{Q} is the internal heating rate per unit mass, and \hat{c}_p is the specific heat at constant pressure.

According to the laboratory experiments on silicate rock deformation, the viscosity of the Earth's mantle depends on various parameters such as temperature, pressure, stress, and so on [12]. Among them, temperature dependence is the most dominant factor. Here we assume that viscosity μ depends only on temperature;

$$\mu(T) = \exp[-E(T - T_{bot})]. \quad (11)$$

The viscosity contrast across the spherical shell is defined by $\gamma_\mu \equiv \mu(T_{top})/\mu(T_{bot}) = \exp(E)$. The mechanical boundary conditions at the top and bottom surface are impermeable and stress-free. The boundary conditions for T are fixed; $T_{bot} = 1$ and $T_{top} = 0$.

3.2. Steady state convection

The thermal convection in the spherical shell with infinite Prandtl number has two stable solutions with polyhedral symmetry when the Rayleigh number is low. The two solutions are found by linear theory and confirmed by numerical simulations [13]: One solution is a convection with the tetrahedral symmetry which has four upwellings; the other has the cubic

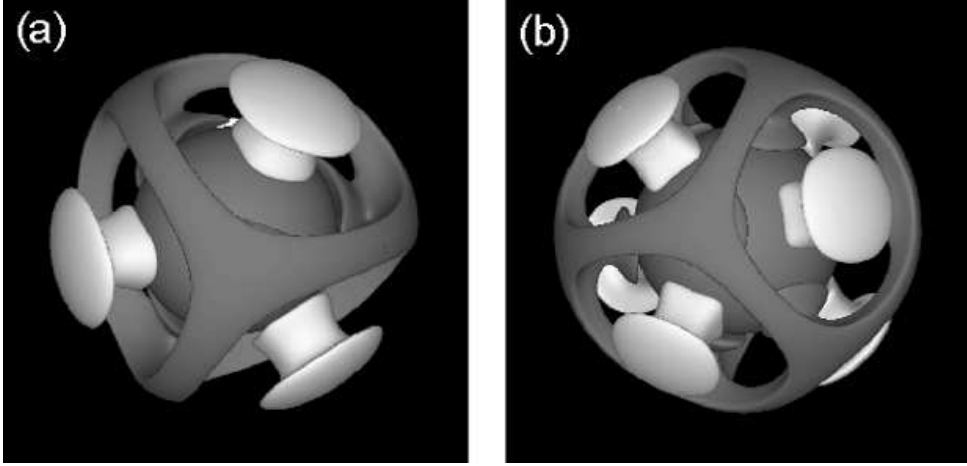


Figure 4. The iso-surface of the residual temperature δT (the deviation from horizontally averaged temperature at each depth) started from the initial condition of (a) the tetrahedral and (b) the cubic symmetries. The Rayleigh number is $Ra = 10^4$. Blue and Yellow iso-surfaces indicate $\delta T = -0.125$ and $\delta T = 0.150$, respectively. Red spheres indicate the bottom of the mantle with fixed temperature.

symmetry with six upwellings. To confirm these symmetric solutions and their stabilities, we performed two simulations with different initial conditions of temperature field; $T(r, \theta, \phi) = T_{cond}(r) + T_{prtb}(r, \theta, \phi)$, where $T_{cond}(r)$ is the purely conductive profile, $\nabla^2 T_{cond}(r) = 0$, with the thermal boundary conditions given above. The perturbation term $T_{prtb}(r, \theta, \phi)$ is given by,

$$T_{prtb}(r, \theta, \phi) = 0.1 Y_3^2(\theta, \phi) \sin \pi(r - r_0), \quad (12)$$

for the tetrahedral symmetric solution, and

$$T_{prtb}(r, \theta, \phi) = 0.1 \left\{ Y_4^0(\theta, \phi) + \frac{5}{7} Y_4^4(\theta, \phi) \right\} \sin \pi(r - r_0), \quad (13)$$

for the cubic symmetric solution, where $Y_\ell^m(\theta, \phi)$ is the normalized spherical harmonic functions of degree ℓ and order m . Fig. 4 shows the steady state convection pattern with the tetrahedral and cubic symmetries. We have performed benchmark tests with previously reported numerical mantle convection codes that employed various numerical schemes. In spite of the differences of the discretization methods, numerical techniques, and number of grid points among the codes, we found that the calculated values such as the Nusselt number obtained by our Yin-Yang mantle code agree well with previous calculations within a few percent.

3.3. Time-dependent convection

The Earth's mantle is obviously in a time-dependent convection under a very high Rayleigh number ($Ra \geq 10^6$) and with internal heating ($H \leq 20$). When $Ra = 10^5$, the convection pattern becomes weakly time-dependent, and the geometrical symmetry is broken. Fig. 5 shows the thermal structures of the mantle convection when $Ra = 10^7$ which is characteristic of the Earth's mantle. Without internal heating, the thermal structure is strongly time-dependent, driven by narrow, cylindrical upwelling (hot) plumes surrounding by a network of long downwelling (cold) sheets (Fig. 5a). This feature is in contrast with the convective feature at low Rayleigh number ($Ra < 10^5$) where the convection is nearly steady state (Fig. 4). On the other hand, when the

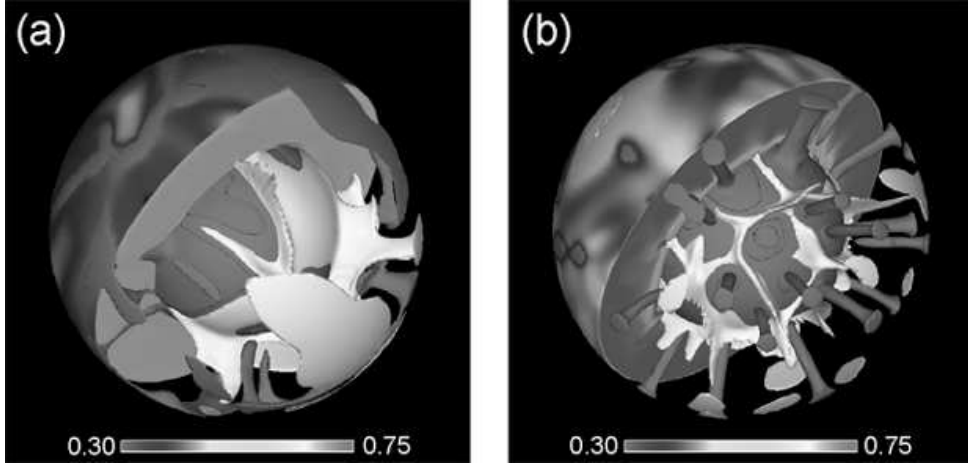


Figure 5. The iso-surface of the temperature T and the residual temperature δT for the cases of (a) $H = 0$ and (b) $H = 20$. The Rayleigh number is $Ra = 10^7$. Iso-surfaces on the half spherical shell indicate the temperature (see color bars). Blue and Yellow iso-surfaces indicate $\delta T = \pm 0.1$, respectively. Red spheres indicate the bottom of the mantle with fixed temperature.

internal heating is taken into account ($H = 20$), the convective feature is dominated by the short-wavelength structure with numerous quasi-cylindrical downwellings spaced relatively close together. The downwellings are surrounded by a broad and diffuse upwelling of hotter fluid (Fig. 5b). We have found that internal heating has a strong influence on the scale and structure of the mantle convection, especially on the shape of downwellings.

The convection pattern is also drastically changed by taking the viscosity variation into account. Fig. 6 shows the thermal structures of the mantle convection with temperature-dependent viscosity at $Ra = 10^7$ and $H = 0$. When the temperature dependence of viscosity is rather moderate (the viscosity contrast across the convecting shell γ_μ is 10^3 – 10^4), the convection

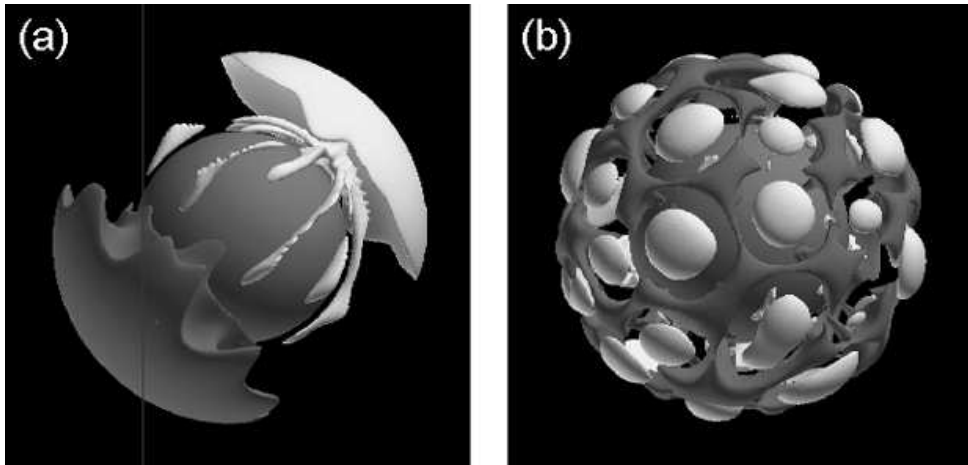


Figure 6. The iso-surface of the residual temperature for the cases of (a) $\gamma_{\mu} = 10^4$ ($E = 9.210$) and (b) $\gamma_{\mu} = 10^6$ ($E = 13.816$). Blue and Yellow iso-surfaces indicate (a) $\delta T = \pm 0.25$ and $\delta T = \pm 0.10$, respectively. Red spheres indicate the bottom of the mantle with fixed temperature.

has long-wavelength thermal structure with a mobile, stiff layer, or, “sluggish-lid” along the cold top surface of the mantle. When $Ra = 10^7$ and $\gamma_\mu = 10^4$, the convection pattern comes to be dominated by the degree-one pattern; the one cell structure that consists of a pair of cylindrical downwelling plume and cylindrical upwelling plume (Fig. 6a). On the other hand, the convective flow pattern that belongs to the “stagnant-lid” regime emerges when $\gamma_\mu \geq 10^5$. The stagnant-lid, which is an immobile, stiff layer, prevents the heat flux through the top boundary and leads to a small temperature difference in the mantle below the lid. Convection under the stagnant-lid is characterized by numerous, small-scale cylindrical plumes surroundings sheet-like downwelling (Fig. 6b). We have found that the variable viscosity with temperature dependence induces drastic effects on the mantle convection pattern.

4. Application to geodynamo simulation

The magnetic compass points to the north since the Earth is surrounded by a dipolar magnetic field. It is broadly accepted that the geomagnetic field is generated by a self-excited electric current in the Earth’s core, The inner core is iron in solid state, and the outer core is also iron but in liquid state due to the high temperature of the planetary interior. The electrical current is generated by magnetohydrodynamic (MHD) dynamo action—the energy conversion process from flow energy into magnetic energy—of the liquid iron in the outer core. In the last decade, computer simulation has emerged as a central research method for geodynamo study [14].

In this section, we show the application of the Yin-Yang grid to the geodynamo simulation with a special emphasize on the code parallelization and sustained performance achieved by the Earth Simulator. We consider a spherical shell vessel bounded by two concentric spheres. The inner sphere of radius $r = r_i$ denotes the inner core and the outer sphere of $r = r_o$ denotes the core-mantle boundary. An electrically conducting fluid is confined in this shell region. Both the inner and outer spherical boundaries rotate with a constant angular velocity $\boldsymbol{\Omega}$. We use a rotating frame of reference with the same angular velocity. There is a central gravity force in the direction of the center of the spheres. The temperatures of both the inner and outer spheres are fixed; hot (inner) and cold (outer). When the temperature difference is sufficiently large, a convection motion starts when a random temperature perturbation is imposed at the beginning of the calculation. At the same time an infinitesimally small, random “seed” of the magnetic field is given.

The system is described by the following normalized MHD equations:

$$\frac{\partial \rho}{\partial t} = -\nabla \cdot \mathbf{f}, \quad (14)$$

$$\frac{\partial \mathbf{f}}{\partial t} = -\nabla \cdot (\mathbf{v}\mathbf{f}) - \nabla p + \mathbf{j} \times \mathbf{B} + \rho \mathbf{g} + 2\rho \mathbf{v} \times \boldsymbol{\Omega} + \mu(\nabla^2 \mathbf{v} + \frac{1}{3}\nabla(\nabla \cdot \mathbf{v})), \quad (15)$$

$$\frac{\partial p}{\partial t} = -\mathbf{v} \cdot \nabla p - \gamma p \nabla \cdot \mathbf{v} + (\gamma - 1)K\nabla^2 T + (\gamma - 1)\eta \mathbf{j}^2 + (\gamma - 1)\Phi, \quad (16)$$

$$\frac{\partial \mathbf{A}}{\partial t} = \mathbf{v} \times \mathbf{B} + \eta \nabla^2 \mathbf{A}, \quad (17)$$

with

$$\begin{aligned} p &= \rho T, & \mathbf{B} &= \nabla \times \mathbf{A}, & \mathbf{j} &= \nabla \times \mathbf{B}, & \mathbf{g} &= -g_0/r^2 \hat{\mathbf{r}}, \\ \nabla \cdot \mathbf{B} &= 0, & \Phi &= 2\mu \left(e_{ij} e_{ij} - \frac{1}{3}(\nabla \cdot \mathbf{v})^2 \right), & e_{ij} &= \frac{1}{2} \left(\frac{\partial v_i}{\partial x_j} + \frac{\partial v_j}{\partial x_i} \right). \end{aligned} \quad (18)$$

Here the mass density ρ , pressure p , mass flux density \mathbf{f} , magnetic field’s vector potential \mathbf{A} are the basic variables in the simulation. Other quantities; magnetic field \mathbf{B} , electric current density \mathbf{j} , and electric field \mathbf{E} are treated as subsidiary fields. The ratio of the specific heat γ , viscosity

Table 1. Specifications of the Earth Simulator.

Peak performance of arithmetic processor (AP)	8 Gflops
Number of AP in a processor node (PN)	8
Total number of PN	640
Total number of AP	8 AP \times 640 PN = 5120
Shared memory size of PN	16 GB
Total peak performance	8 Gflops \times 5120 AP = 40Tflops
Total main memory	10 TB
Inter-node data transfer rate	12.3 GB/s \times 2

μ , thermal conductivity K and electrical resistivity η are assumed to be constant. The vector \mathbf{g} is the gravity acceleration and $\hat{\mathbf{r}}$ is the radial unit vector; g_0 is a constant. We normalize the quantities as follows: The radius of the outer sphere $r_o = 1$; the temperature of the outer sphere $T(1) = 1$; and the mass density at the outer sphere $\rho(1) = 1$. The temperature on the inner and outer spheres are fixed. The boundary condition for the velocity is rigid;

$$\mathbf{v} = 0, \quad \text{at } r = r_i, 1. \quad (19)$$

The boundary condition for the magnetic field is given by

$$B_\theta = B_\phi = 0, \quad \text{at } r = r_i, 1. \quad (20)$$

We will consider the improvement of this rather artificial boundary condition into more realistic one in the end of this section. The spatial derivatives in the above equations are discretized by the second-order central finite difference method on the Yin-Yang grid. The fourth-order Runge-Kutta method is used for the temporal integration. Initially, both the convection energy and the magnetic energy are negligibly small. For geodynamo study, it is necessary to follow the time development of the MHD system until the thermal convection flow and the dynamo-generated magnetic field are both sufficiently developed and saturated.

We developed this Yin-Yang based geodynamo simulation code for the Earth Simulator by converting our previous geodynamo code, which was based on the traditional latitude-longitude grid, into the Yin-Yang grid. We have found that the code conversion from our previous latitude-longitude based code into the new Yin-Yang based code is straightforward and rather easy. Our experience with the rapid and easy conversion from latitude-longitude code into Yin-Yang code would be encouraging for others who have already developed codes that are based on latitude-longitude grids in the spherical coordinates, and who are bothered by numerical problems and inefficiency caused by the pole singularity. We would like to suggest that they try the Yin-Yang grid.

Since the Yin grid and Yang grid are identical, dividing the whole computational domain into a Yin grid part and a Yang grid part is not only natural but also efficient for parallel processing. In addition to this Yin-and-Yang division, further domain decomposition within each grid is applied to for the massively parallel computation on the Earth Simulator.

The Earth Simulator, whose hardware specifications are summarized in Table 1 has three different levels of parallelization: Vector processing in each arithmetic processor (AP); shared-memory parallelization by 8 APs in each processor node (PN); and distributed-memory parallelization by PNs.

In our Yin-Yang dynamo code, we apply vectorization in the radial dimension of the three-dimensional (3D) arrays for physical variables. The radial grid size is 255 or 511, which is just below the size (or doubled size) of the vector register of the Earth Simulator (256) to avoid bank conflicts in the memory. We use MPI both for the inter-node (distributed memory) parallel processing and for the intra-node (shared memory) parallel processing. This approach is called “flat-MPI” parallelization.

As we mentioned above, we first divide the whole computational domain into two identical parts that correspond to the Yin grid and Yang grid shown in Fig. 3(a). (Therefore, the total number of processes is always even.) For further parallelization within each component grid, we applied the two-dimensional decomposition in the horizontal space, colatitude θ and longitude ϕ . More details on the parallelization of this code is described in [15].

The best performance of the Yin-Yang geodynamo code with the flat MPI parallelization is 15.2 Tflops. This performance is achieved by 4096 processors (512 nodes) with the total grid size of 511(radial) \times 514(latitudinal) \times 1538(longitudinal) \times 2(Yin and Yang). Since the theoretical peak performance of 4096 processors is 4096×8 Gflops = 32.8Tflops, we have achieved 46% of peak performance in this case. The average vector length is 251.6, and the vector operation ratio is 99%. The high performance of the Yin-Yang dynamo code is a direct consequence of the simple and symmetric configuration design of the Yin-Yang grid: It makes it possible to minimize the communication time (10%) between the processes in the horizontal directions, and enables optimum vector processing (with 99% of operation ratio) in the radial direction in each process.

Before concluding this section, we briefly describe our recent improvement of the Yin-Yang geodynamo code. We have improved the boundary condition denoted by eq. (20) of the magnetic field into more realistic one, i.e., so called vacuum boundary condition. In this boundary condition, the magnetic field generated by the MHD dynamo in the outer core ($r \leq 1$) is smoothly connected to the magnetic field \mathbf{B}_v of the outer region $r > 1$ that is assumed to be an insulator;

$$\nabla \times \mathbf{B}_v = 0, \quad \text{for } r > 1. \quad (21)$$

Therefore, the \mathbf{B}_v is written by a scalar function ψ ,

$$\mathbf{B}_v = -\nabla\psi, \quad \text{for } r > 1, \quad (22)$$

where, from $\nabla \cdot \mathbf{B}_v = 0$, ψ satisfies the potential equation

$$\nabla^2\psi = \left[\frac{1}{r^2} \frac{\partial}{\partial r} \left(r^2 \frac{\partial}{\partial r} \right) + \frac{1}{r^2 \sin \theta} \frac{\partial}{\partial \theta} \left(\sin \theta \frac{\partial}{\partial \theta} \right) + \frac{1}{r^2 \sin^2 \theta} \frac{\partial^2}{\partial \phi^2} \right] \psi = 0, \quad \text{for } r \geq 1 \quad (23)$$

The boundary condition of ψ at $r = 1$ is given by $-\nabla\psi(r = 1) = B_r(r = 1)$, where $B_r(r = 1)$ is determined from the dynamo region ($r \leq 1$). Other component of the magnetic field at the surface $B_\theta(r = 1)$ and $B_\phi(r = 1)$ are determined by the solution of eq. (23). In order to solve this boundary value problem, we first apply a coordinate transformation of r .

$$r \rightarrow \zeta = 1/r. \quad (24)$$

The equation (23) is converted into the following form

$$\left[\zeta^2 \frac{\partial^2}{\partial \zeta^2} + \frac{1}{\sin \theta} \frac{\partial}{\partial \theta} \left(\sin \theta \frac{\partial}{\partial \theta} \right) + \frac{1}{\sin^2 \theta} \frac{\partial^2}{\partial \phi^2} \right] \psi = 0, \quad \text{for } 0 \leq \zeta \leq 1 \quad (25)$$

The problem to solve eq. (23) *outside* a unit sphere $r \geq 1$ is now converted into the problem to solve eq. (25) *inside* a unit sphere $\zeta \leq 1$. The boundary condition of ψ at the origin $\zeta = 0$ is given by $\psi(\zeta = 0) = 0$ since $\psi(r = \infty) = 0$.

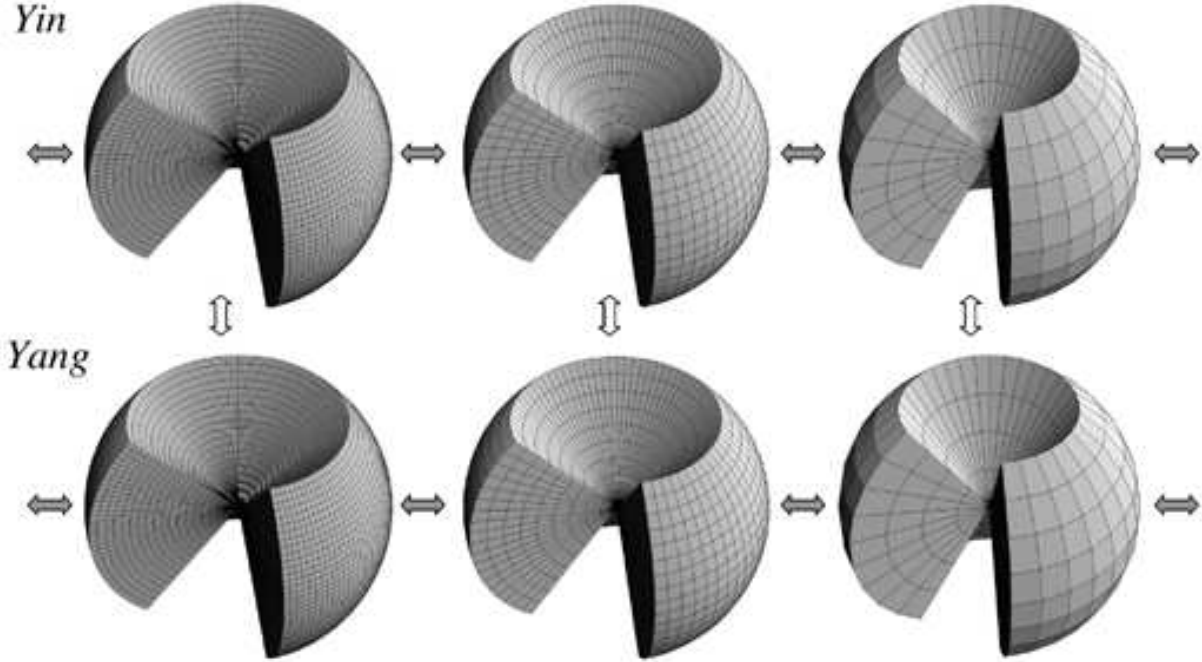


Figure 7. The Yin-Yang multigrid method for the solution of the vacuum magnetic field potential ψ . The full approximation storage algorithm is used. The horizontal boundary values of the Yin and Yang grids for the overset are determined by the mutual interpolation (white arrows) at the every grid level in the V-cycle of the multigrid method (gray arrows).

To solve eq. (25), we apply the multigrid method [16], which is practically the optimal way to solve this kind of boundary value problem. The base grid system is the Yin-Yang grid defined in the full spherical region including the origin. See Fig. 7. We adopt the full approximation storage algorithm of the multigrid method. The Jacobi method is used as the smoother. The V-cycle is repeated for a couple of times until we get the convergence. The internal boundary condition of each component grid (Yin and Yang) are set by mutual bi-cubic interpolation at every grid level as indicated by white arrows in Fig. 7. Although, the code is not parallelized yet, its flat-MPI parallelization will be straightforward. We have combined this non-parallelized Yin-Yang multigrid solver of the vacuum potential ψ with the non-parallel version of the Yin-Yang geodynamo code. We have found that the vacuum field condition has been successfully implemented by this multigrid potential solver with almost the same computational cost (CPU time) as with the MHD solver part. This is a very promising result for further development.

5. Summary

We have developed a new spherical overset grid, “Yin-Yang grid”, for geophysical simulations. The Yin-Yang grid is constructed from a dissection of a sphere into two identical and complementary pieces. Among various possible overset grids over a sphere, we believe that the Yin-Yang grid is the simplest and the most powerful especially on massively parallel computers from the following reasons:

- It is an orthogonal system, since it is a part of the latitude-longitude grid.
- The grid spacing is quasi-uniform, since we picked up only the low latitude region of the latitude-longitude grid.

- The metric tensors are simple and analytically known, since it is defined based on the spherical polar coordinates.
- Routines for the fluid (or MHD) solver can be recycled twice, since Yin and Yang are identical.
- Routines for mutual interpolations of the overset grid borders can also be recycled twice, since Yin and Yang are complementary.
- Parallelization is easy and efficient, since the domain decomposition is straightforward.

We have developed finite difference codes of the geodynamo simulation and the mantle convection simulation on the Yin-Yang grid. The Yin-Yang geodynamo code has achieved 15.2 Tflops with 4096 processors on the Earth Simulator. This represents 46% of the theoretical peak performance. By the Yin-Yang mantle code, we can carry out realistic mantle convection simulations under the Rayleigh number of 10^7 , including strongly temperature-dependent viscosity whose contrast reaches up to 10^6 .

In the Earth Simulator Center, the Yin-Yang grid is also applied to advanced general circulation modes of the atmosphere and ocean [17, 18, 19].

Acknowledgments

The authors would like to thank Prof. Tetsuya Sato, the director-general of the Earth Simulator Center, for instructive discussions and Dr. Masanori Kameyama for useful comments on the application of the multigrid method to the Yin-Yang grid. All the simulations were performed on the Earth Simulator.

References

- [1] Chesshire G and Henshaw W D 1990 Composite overlapping meshes for the solution of partial differential equations *J. Comput. Phys.* **90** 1–64
- [2] Steger J L, Dougherty F C and Benek J A 1983 A Chimera grid scheme *Proc. Advances in Grid Generation* ed K N Ghia and U Ghia (Houston) ASME FED vol 5 pp 59–69
- [3] Steger J L 1982 On application of body conforming curvilinear grids for finite difference solution of external flow *Numerical Grid Generation* ed J F Thomposon (Amsteram: North-Holland) pp 295–316
- [4] Phillips N A 1957 A map projection system suitable for large-scale numerical weather prediction *J. Meteor. Soc. Japan* **75** 262–7
- [5] Phillips N A 1959 Numerical integration of the primitive equations on the hemisphere *Month. Weather Rev.* **87** 333–45
- [6] Browning G L, Hack J J and Swarztrauber P N 1989 A comparison of three numerical methods for solving differential equations on the sphere *Month. Weath. Rev.* **117** 1058–75
- [7] Ronchi C, Iacono R and Paolucci P S 1996 The “cubed sphere”: A new method for the solution of partial differential equations in spherical geometry *J. Comput. Phys.* **124** 93–114
- [8] Hernlund J W and Tackley P J 2003 Three-dimensional spherical shell convection at infinite Prandtl number using the ‘cubed sphere’ method *Proc. Second MIT Conference on Computational Fluid and Solid Mechanics* (Cambridge)
- [9] Dudhia J and Bresch J F 2002 A global version of the PSU-NCAR mesoscale model *Month. Weather Rev.* **130** 2989–3007
- [10] Yoshida M and Kageyama A 2004 Application of the Yin-Yang grid to a thermal convection of a Boussinesq fluid with infinite Prandtl number in a three-dimensional spherical shell *Geophys. Res. Lett.* **31** L12609
- [11] McKenzie D P, Roberts J M and Weiss N O 1974 Convection in the earth’s mantle: Towards a numerical simulation. *J. Fluid Mech.* **62** 465–538
- [12] Turcotte D L and Schubert G 2002 *Geodynamics* (Cambridge: Cambridge Univ. Press)
- [13] Bercovici B, Schubert G, Glatzmaier G A and Zebib A 1989 Three dimensional thermal convection in a spherical shell *J. Fluid Mech.* **206** 75–104
- [14] Kono M and Roberts P H 2002 Recent geodynamo simulations and observations of the geomagnetic field *Rev. Geophys.* **40** 1013
- [15] Kageyama A, Kameyama M, Fujihara S, Yoshida M, Hyodo M and Tsuda Y 2004 A 15.2 Tflops simulation of geodynamo on the earth simulator *Proc. ACM/IEEE Supercomputing Conference SC2004* (Pittsburgh)

- [16] Wesseling P 2004 *An Introduction to Multigrid Methods* (Philadelphia: R. T. Edwards Inc., John Wiley & Sons Ltd., 1992. Corrected Reprint)
- [17] Takahashi K et al 2004 Development of nonhydrostatic coupled ocean-atmosphere simulation code on the earth simulator *Proc. 7th International Conference on High Performance Computing and Grid in Asia Pacific Region* (Omiya) pp 487–94
- [18] Komine K, Takahashi K and Watanabe K 2004 Development of a global non-hydrostatic simulation code using yin-yang grid system *Proc. 2004 workshop on the solution of partial differential equations on the sphere* (Yokohama) pp 67–9
- [19] Takahashi K 2004 Development of nonhydrostatic coupled ocean-atmosphere simulation code *Annual Report of the Earth Simulator for Fiscal year 2003* pp 63–7